Journal of Physics D: Applied Physics

PAPER

Demonstration of compensated *n*-type scandium nitride Schottky diodes

To cite this article: Dheemahi Rao *et al* 2023 *J. Phys. D: Appl. Phys.* **56** 074004

IOP Publishing Journal of Physics D: Applied Physics

J. Phys. D: Appl. Phys. **56** (2023) 074004 (9pp) https://doi.org/10.1088/1361-6463/acb3da

Demonstration of compensated *n*-type scandium nitride Schottky diodes

Dheemahi Rao[1,2], **Shashidhara Acharya**[2] and **Bivas Saha**[1,2,3,*]

[1] Chemistry and Physics of Materials Unit, Jawaharlal Nehru Centre for Advanced Scientific Research, Bangalore 560064, India
[2] International Centre for Materials Science, Jawaharlal Nehru Centre for Advanced Scientific Research, Bangalore 560064, India
[3] School of Advanced Materials (SAMat), Jawaharlal Nehru Centre for Advanced Scientific Research, Bangalore 560064, India

E-mail: bsaha@jncasr.ac.in and bivas.mat@gmail.com

Received 9 November 2022, revised 3 January 2023
Accepted for publication 17 January 2023
Published 31 January 2023

Abstract

Scandium nitride (ScN) is an emerging group III-B transition metal pnictide and has been studied extensively for its thermoelectric properties, as interlayers for defect-free GaN growth, in epitaxial metal/semiconductor superlattices, and recently for its polaritonic and optoelectronic synaptic functionalities. However, to realize the full potential of its semiconducting properties in electronic, thermionic, and optoelectronic device applications, it is necessary to develop Schottky diodes of ScN that are missing thus far. Here we show Schottky diodes of ScN with elemental metals such as silver (Ag) and gold (Au). As-deposited ScN thin films exhibit a high electron concentration in the (1–4) $\times$ 10^{20} cm^{-3} range due to unintentional oxygen doping. These excess electrons are compensated by Mg hole doping, leading to a wider depletion region at the metal/ScN interface for activated electronic transport. Current–voltage (I–V) characteristics show the rectification nature in ScN/Ag and ScN/Au diodes, and the barrier heights of 0.55 $\pm$ 0.05 eV and 0.53 $\pm$ 0.06 eV, respectively, are obtained. Interface annealing with time and temperature results in a slight increase in the forward junction potential. The capacitance–voltage (C–V) measurements also revealed the presence of interface trap states. The demonstration of Schottky diodes marks an important step in realizing the full potential of ScN in electronic, thermionic, and optoelectronic devices.

Supplementary material for this article is available online

Keywords: Scandium nitride, Schottky diodes, transition metal nitrides, fermi level pinning, interface trap states

(Some figures may appear in colour only in the online journal)

1. Introduction

Transition metal nitrides (TMNs) are an emerging family of materials and have been researched extensively in recent years for various applications. Traditionally, TMNs are utilized in hard coating and tribology industries due to their corrosion resistant high hardness, high melting temperature, and for their excellent structural/chemical stability [1–4]. However, over the last ten years, TMNs have demonstrated novel applications in many present-day research fields, such as plasmonics, catalysis, hot carrier solar cells, etc. For example, metallic TMNs such as TiN and HfN (ZrN) have emerged as alternative plasmonic materials to Au and Ag for visible and

* Author to whom any correspondence should be addressed.

near-ultraviolet spectral range applications, respectively [5–7]. Similarly, ZrN exhibited comparable or even better catalytic properties compared to Pt for oxygen reduction reaction [8]. Scandium nitride (ScN) is one of the most famous semiconducting TMN and exhibits a high hardness (∼24 GPa), high melting temperature (∼2600 °C), and is stable at ambient temperature and pressure [9–12]. Unlike its wurtzite group III-A nitride counterparts, ScN exhibits rocksalt crystal structure, indirect electronic $\Gamma - X$ bandgap of ∼0.9 eV and a direct $\Gamma - \Gamma$ gap of 2.2 eV [10, 13–16]. Due to this fundamental difference in the crystal and electronic structure, ScN is attractive for applications where most traditional group III-A semiconductors do not work satisfactorily.

In terms of the electronic properties, ScN thin films deposited with ultrahigh vacuum (UHV) magnetron sputtering or with molecular beam epitaxy are highly degenerate and exhibit an *n*-type carrier concentration in the (1–4) $\times$ 10^{20} cm^{-3} range at room temperature [17–20]. Such large carrier concentration in ScN arises from the presence of oxygen as impurity and nitrogen vacancies during the growth process [21–23]. Due to such high carrier concentration and high electron mobility of ∼80–120 cm^2 V^{-1}s^{-1}, ScN thin films exhibit a high thermoelectric power factor of (2–3.5) $\times$ 10^{-3} W mK^{-2} in the 500 °C–600 °C range [18, 24, 25]. However, the thermal conductivity of ScN (∼15 W mK^{-1} at 300 °C) is rather high that results in an overall moderate thermoelectric *figure-of-merit (zT)* of ∼0.15–0.30 at 500 °C [18, 25]. Several strategies, such as alloying ScN with other heavy metal nitrides (such as NbN, CrN, etc) and ion-beam irradiation have been employed to reduce the thermal conductivity and increase ZT [26–30]. Solid solution alloys of ScN with wurtzite III-nitride semiconductors such as $Al_xSc_{1-x}N$, $Ga_xSc_{1-x}N$ have also demonstrated high *c*-axis piezoelectric coefficient and are actively researched for resonators and bulk/surface acoustic wave devices in recent times [31–34].

Since most metals belonging to the TMN family such as ZrN, TiN, and HfN exhibit the same crystal structure and a closely matched lattice constant with ScN, epitaxial metal/semiconductor superlattices are deposited with ScN as the semiconducting component [35, 36]. Such metal/semiconductor metamaterials have demonstrated optical metamaterial properties and currently researched for thermionic energy conversion [37, 38]. Similarly, because of their lattice-matched interface, (111) ScN interlayers have been used successfully to grow dislocation and defect-free (0001) GaN [39, 40]. The high carrier concentration of ScN is further leveraged to excite low-loss and high-quality plasmon and phonon polaritons in the near and far infrared (IR) spectral ranges, respectively. With changes in the *n*-type carrier concentration, epsilon near zero resonance starting from 1.8 μm to 2.4 μm spectral range is achieved [41]. The polar semiconducting nature of ScN also leads to a highly reflecting Reststrahelen band spanning from 14.6 μm to 27.8 μm and far IR light-matter coupling through the excitation of surface phonon polariton modes [41]. Photoconductivity and carrier relaxation in ScN also show intriguing properties in as-deposited and hole-doped films. The positive and negative photoconductivity in ScN is utilized to demonstrate optoelectronic artificial synapses with inhibitory and excitatory synaptic junctions. Such ScN-based optoelectronic synapses have demonstrated short-term memory and long-term memory, paired pulse facilitation and depression, Hebbian learning and logic gate operation, etc [42].

While these exciting developments in ScN research have attracted significant attention, the possibility of ScN-based electronic devices has not been explored much. One of the fundamental steps in this direction would be the demonstration of ScN-based Schottky junction diodes that will rectify current across the ScN/metal interface. Demonstrating Schottky diodes and associated rectifying electronic transport is also essential for ScN's potential applications in thermionic, electronic, and optoelectronic devices and its integration in modern integrated circuits. However, one of the major challenges for achieving Schottky or *pn*-junction diodes in ScN has been its high electron concentration ((1–4) $\times$ 10^{20} cm^{-3}). Such semimetal or degenerate semiconducting nature helped ScN to achieve high thermoelectric and plasmon-polaritonic performances, but prevented the development of diodes and thermionic devices. Such high electron concentration generally led to the formation of Ohmic contacts with metal due to the narrow depletion width. Previously, a few metal (Ti, Ni, Cu, Al, Pd) contacts were deposited on ScN thin film, and their junction characteristics were found to be non-rectifying [43]. Since the ScN films were deposited at low temperatures, large dislocation density and millimeter-sized contacts could have also contributed to the non-rectifying electronic nature. However, rectification was achieved in ScN/GaN and *n*-ScN/*p*-Si barriers, where a significant depletion layer is formed at the semiconductor/semiconductor interface [44, 45]. Fortunately, Mg-hole doping has been used successfully to compensate for the high carrier concentration in ScN [30, 46, 47]. Through Mg-hole doping, *n*-type films with carrier concentrations as low as 2 $\times$ 10^{18} cm^{-3} have been achieved [46]. Such films with lowered electron concentration can be used for devising a Schottky barrier.

Therefore, with the motivation to develop ScN-based electronic devices, we show the fabrication of ScN Schottky diodes with elemental metals such as silver (Ag) and gold (Au) in this work. Mg is doped to reduce the electron concentration and achieve a sufficiently wide depletion layer. To reduce the leakage through the dislocations, ScN films are deposited at high growth temperatures (∼800 °C) and metal contacts with sizes as small as 70 μm are used. The Ag/ScN and Au/ScN diodes show current rectification behavior and barrier heights of 0.55 $\pm$ 0.05 eV and 0.53 $\pm$ 0.06 eV, respectively. Though the performance of the diodes can be improved further with the optimization of material and fabrication techniques, this work marks the first demonstration of a significant rectification in the ScN/metal Schottky interface.

2. Methods

Mg-doped ScN thin films are deposited with a magnetron sputtering in an UHV (base pressure of 1 $\times$ 10^{-9} Torr.) chamber on (001) MgO substrates. The substrates are sonicated in acetone and methanol and dried with nitrogen prior to loading into the load lock chamber. The substrates are heated to 800 °C and held for 30 min to ensure uniform heating and complete desorption of surface impurities before the growth. Sc and Mg are co-sputtered at 125 W and 6 W, respectively, with $Ar:N_2$ flow rate of 9:2 standard cubic centimeters per minute (sccm.) for three hours to achieve a film thickness of 230 nm. Due to the Mg-hole doping, films exhibit a room temperature electron concentration of 4×10^{18} cm^{-3}, mobility of 15 cm^2 V^{-1}s^{-1}, and resistivity of 108 mΩ cm.

The films are then dipped in dilute HCl for 60 s and coated with photoresist immediately for patterning circular contacts of different diameters using optical lithography. As dilute HCl etches ScN at the rate of about 3 nm min^{-1}, the possible surface oxide should be removed with this process. Approximately 40 nm thick Ag and Au are deposited on the film with a high-vacuum thermal evaporator, and the sample is subsequently dipped in acetone for lift-off. Circular contacts with diameters 70, 100, 200, 300, 500, and 700 μm are fabricated. Indium is pressed onto the ScN film to form about 1 mm circular Ohmic contact. All the electrical measurements are performed across the lateral contacts (as shown in the insets in figure 2) in the probe station attached with Keithley 4200.

3. Results and discussions

Carrier transport in a metal/semiconductor Schottky junction, in general, can take place through three mechanisms, thermionic emission (TE), thermionic field emission (TFE) or field emission (FE), depending on the nature of the barrier and the energy of the carriers (figure 1(a)). For a given carrier concentration (N), carrier effective mass (m^*) and dielectric constant (ϵ_s) of the semiconductor, the underlying transport mechanism can be determined by an estimation of E_{00}, calculated with the following expression,

$$E_{00} = \frac{q\hbar}{2}\sqrt{\frac{N}{m^*\epsilon_s}}$$

where, q and $\hbar$ are the charge of an electron and reduced Plank's constant, respectively [48]. For ScN, $m^* = 0.39m_0$ and $\epsilon_s = 12.3\epsilon_0$ is used to calculate E_{00} as a function of the electron concentration (see figure 1(b)). To achieve current rectification at the Schottky barrier, the transport should be predominantly TE. It is clear from figure 1(b) that TE can be achieved in ScN when its carrier concentration is reduced to less than 2×10^{18} cm^{-3}. For carrier concentration of more than 2×10^{18} cm^{-3}, TFE will occur, and subsequently, at higher electron concentration ($>\sim 1 \times 10^{20}$ cm^{-3}), FE would dominate. Since as-deposited ScN thin films exhibit an electron concentration in the (1–4) $\times 10^{20}$ cm^{-3} range, for the demonstration of Schottky diodes, it is necessary to reduce the carrier concentration. Therefore, Mg-hole doping is used to reduce the electron concentration in ScN (figure 1(c)). For an Mg-doping concentration of 1.6 atomic %, a low electron concentration of 4×10^{18} cm^{-3} is achieved. The metal/ScN barriers are studied with this low electron concentration n-type ScN. Technically, since Mg concentration is relatively high, $Sc_{0.984}Mg_{0.016}N$ is an alloy. However, Mg does not introduce any energy states within the bandgap or alter the band edges but only compensates the excess electrons [46, 49]. Since Mg acts just like a p-type dopant in ScN, we use the term Mg-doping or hole-doping in the manuscript. Further increase in the Mg-dopant concentration leads to p-type ScN, as shown in figure 1(c).

High-resolution thin film x-ray diffraction (HRXRD) of the $Sc_{0.984}Mg_{0.016}N$ film with 4×10^{18} cm^{-3} electron concentration (see figure 1(d)) reveals epitaxial nominally single-crystalline growth on (001) MgO substrates. Two XRD peaks at 39.96° and 42.91° correspond to the (002) orientation of ScN and MgO, respectively. The lattice constant of $Sc_{0.984}Mg_{0.016}N$ is 4.51 Å, which is practically the same as that of the intentionally undoped-ScN [50]. The HRXRD of undoped ScN is also shown in figure 1(d) for comparison. The (001) planes can be slightly tilted relative to <001> due to dislocations. This spread in crystal plane orientation, mosaicity, is seen as the widening in ω-scan (rocking curve) peak. The ω-scan corresponding to the (002) diffraction peak in ScN (see inset in figure 1(d)) exhibits a full-width-at-the-half-maxima of $\sim$0.73° for both ScN and $Sc_{0.984}Mg_{0.016}N$, suggesting the retention of crystalline quality. The surface comprises square-shaped compact grains, as evidenced in the plan-view field-emission scanning electron microscopy images (figure 1(e)). The atomic-force microscopy image further verifies the Ehrlich–Schwoebel barrier-controlled epitaxial growth mechanism of ScN, as reported previously [51]. The surface rms roughness exhibits a relatively low value of 0.6 nm. The structural characterizations suggest that Mg-hole doping does not degrade the crystalline quality of ScN films, which is extremely important for device performance.

Device current varies linearly with the applied voltage for ScN/indium (In) contact (see figure 2(a)). The linear I–V relation signifies the Ohmic nature of In/ScN interface, even when the electron concentration in ScN is low (4×10^{18} cm^{-3}). On the other hand, a non-linear diode-like I–V characteristic is obtained across Ag/ScN/In and Au/ScN/In junctions. Since, In forms Ohmic contact with ScN, the diode-like I–V is obtained due to the Schottky barrier formation at the Ag/ScN and Au/ScN interfaces. An apparent current rectification is observed when the current passes through the smallest 70 μm Ag and Au contacts, as shown in figures 2(b) and (c), respectively. The reverse current in Ag/ScN Schottky diodes is at least one order of magnitude less than the forward current in the entire voltage range measured here. The current rectification ratio (RR) (ratio of forward current to reverse current at a particular voltage) at 2 V for the Ag/ScN diode is $\sim$60. The reverse leakage current increases at higher voltages lowering the RR to $\sim$25 at 3 V. The reverse leakage current is higher for Au/ScN diode with RR of 3 at 2 V. The forward voltage drop (V_F) for Ag/ScN and Au/ScN is about 1.3 V and 0.9 V, respectively. Though the RR is lower and V_F is higher in comparison to the well-established Schottky diodes of Si and GaN, it is the first time that Schottky diodes are demonstrated in ScN, and a significant rectification is observed [52, 53].

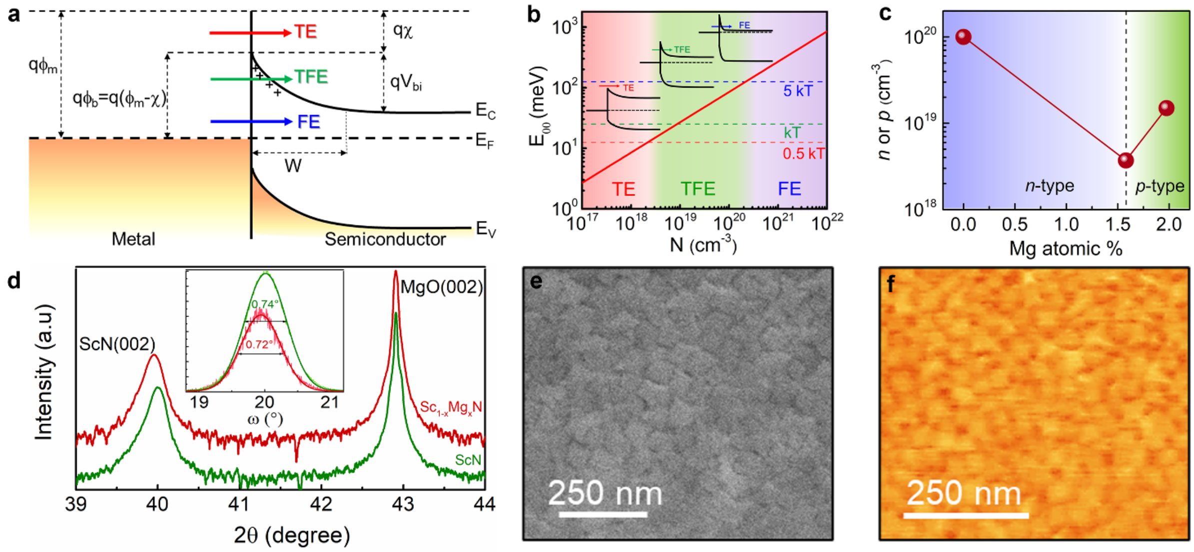

Figure 1. (a) Schematic of metal/semiconductor Schottky barrier across which electron can be transported by field emission (FE), thermionic field emission (TFE) or thermionic emission (TE). (b) The plot of E_{00} for ScN shows which carrier transport mechanism dominates in the Schottky barrier as a function of carrier concentration. The schematic of the change in barrier shape facilitating each carrier transport is also shown. (c) Increasing Mg target power initially reduces the electron concentration to a minimum (4×10^{18} cm^{-3}) and then leads to p-type ScN. (d) The HRXRD shows single crystalline Mg-doped n-ScN (002) oriented growth on (002) MgO. The 0.72° FWHM of the rocking curve in the inset reveals slight mosaicity. (e) Plan-view FESEM image presents the smooth, compact surface with square features arising from its cubic crystal structure. (f) Atomic force microscopy (AFM) image suggests a smooth surface with rms roughness of 0.6 nm.

Careful analysis of the logarithmic plot of forward current characteristics for the Ag/ScN diode shows three regions suggesting different carrier transport mechanisms (see figure 3(a)). In a small range of low voltages (region I), the current varies linearly, and the magnitude of current is also very small. Here, the carrier injection from the metal into the semiconductor is less due to the insufficient voltage to overcome the barrier. In region II, the current rises exponentially due to the TE across the barrier. The barrier height (Φ_b) and the ideality factor (n) can be calculated by fitting the J–V characteristic in this region with the Schottky diode equation (as in the inset in figure 3(a))

$$J = J_0\, e^{\frac{qV}{nkT}}$$

$$\text{Where, } J_0 = A^* T^2 exp\left(-q\Phi_b/kT\right).$$

Here, J_0 is saturation current density, k is Boltzmann's constant, T is absolute temperature, and A^* is effective Richardson coefficient (3.38×10^5 A m^{-2}K^{-2}). The fitting of 70 μm Ag/ScN diode current yields a barrier height of 0.55 ± 0.05 eV and an ideality factor of $\sim$8. The higher ideality factor points to the fact that TE does not solely dominate transport. Additionally, interface inhomogeneity, series resistance, and formation of a layer due to diffusion at the interface also contribute to higher n. Finally, in region III, the current varies as $\sim V^n$ ($n = 2$–3), suggesting the space-charge limited current (SCLC) transport mechanism. The carrier injection overpowers the equilibrium charge distribution at the barrier giving rise to the SCLC regime [54].

The forward I–V characteristic is also analyzed with Cheung method, and the series resistance (R_{series}) of $\sim$5000 Ω is measured (details in SI) [55]. Such a high resistance value is presumably due to the lateral geometry of the contacts that are separated by a few millimeters. With this method, Ag/ScN barrier height and ideality factor are calculated to be 0.53 eV and 7.7, respectively, endorsing the earlier calculations. The effect of R_{series} is evident from the semi-logarithmic plot of the diode current, and R_{series} value of 3930 Ω is extracted (details in SI).

Variations of the I–V characteristics with Ag contact diameter (see figure 3(b)) show that though the diode current varies non-linearly for all metal contact sizes studied here, the rectification decreases for larger contact diameters. Such behavior could be attributed to the increased shunt paths beneath the contacts that allow electron transport without the influence of an effective barrier. The linear fit of reverse leakage current (I_R) at -1 V as a function of contact diameter (see SI) has a slope of nearly two, suggesting that the leakage current is proportional to the area of the contact [56]. Further discussion on the variation of shunt and series resistance with the size of the contacts is included in SI. For such reasons, a smaller contact size is traditionally preferred to demonstrate Schottky diodes in GaN and other materials [57].

The impact of ageing on the diode characteristics is further determined by the I–V measurements at different time intervals after the initial measurement. With time (day 5 and day 14), the Ag/ScN diodes show lower reverse leakage

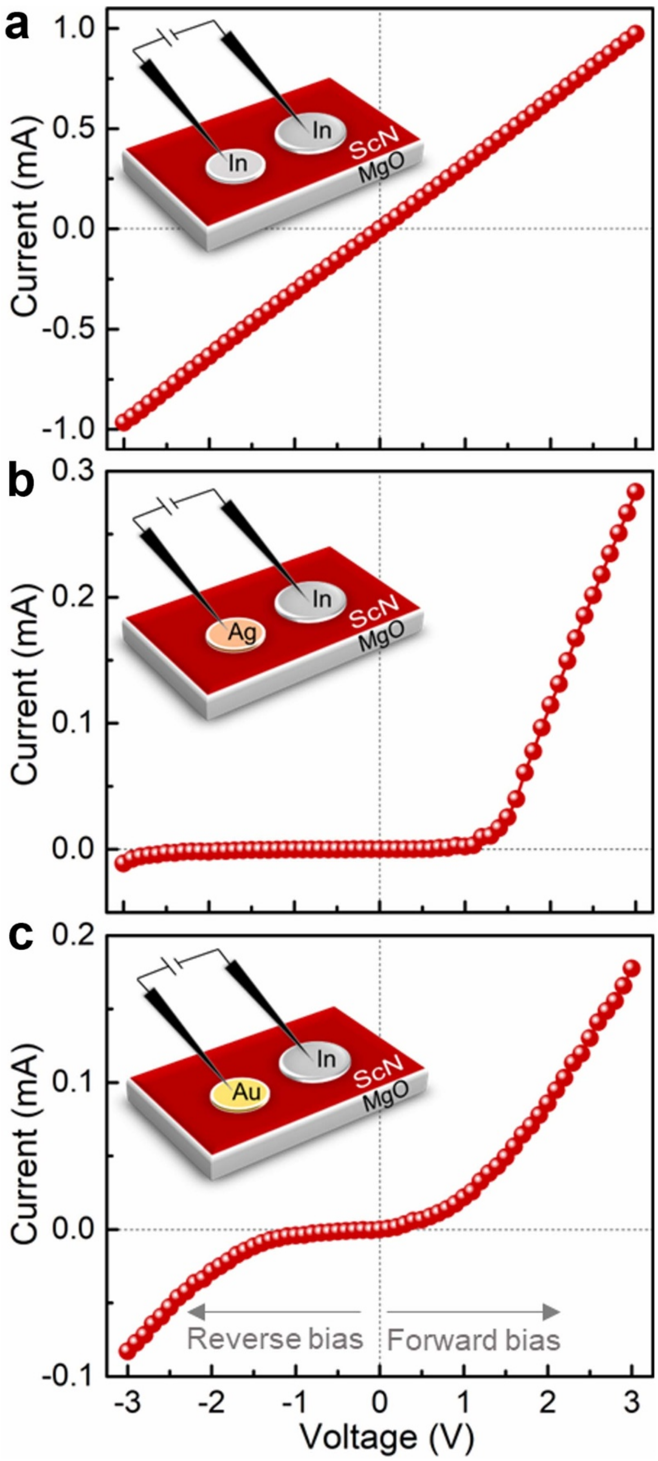

Figure 2. *I–V* characteristic curves of (a) In/ScN, (b) Ag/ScN, and (c) Au/ScN. The linear variation of I with V suggests that In forms Ohmic contact with ScN. Ag and Au form Schottky diodes with rectifying ability. The inset shows the device structure.

current and the rectification increases (see figure 3(c)). Beyond 14 days of timeframe, diode characteristics remain practically the same. This observed phenomenon indicates the possibility of some interfacial reaction that enhances the rectification. Diffusion of Ag or bonding with dangling bonds eventually forms a layer that increases the barrier height and series resistance [58, 59]. Similarly, temperature-dependent *I–V* measurements reveal a slight increase in forward voltage drop and thus the barrier height when heated up to 75 °C (figure 3(d)). The slight increase in barrier height and decrease in ideality factor (see SI) are due to the potential fluctuation and spatial inhomogeneities at the interface, as reported earlier in other Ag/semiconductor barriers [60]. The inset in figure 3(d) shows the decrease in current at 2 V as the temperature increases, implying the barrier modification.

To gain further insight into the diode functionalities, capacitance–voltage (*C–V*) measurements are performed by sweeping DC voltage across the Ag/ScN junction with a superposed 30 mV AC (figure 4(a)). At 100 kHz AC, the capacitance in the reverse bias slightly reduces from 0 to -3 V due to the reverse current leakage. Whereas, in the forward bias, the capacitance steeply drops after $\sim$1.5 V, where the current begins to flow across the barrier. The peak around 0 V in the *C–V* curve is due to the increased capacitance of the interface traps as the depletion layer becomes thin. At higher frequencies, the magnitude of the capacitance is reduced as the contribution from the interface traps reduces; but the nature of the *C–V* remains the same. Variation of capacitance with AC frequency at 0 V and -3 V is presented in figure 4(b). Capacitance under reverse bias is lower than the zero-bias capacitance at lower frequencies due to the voltage response of the interface traps [61]. At higher frequencies (>0.5 MHz), where trap states are not responsive, the capacitance is independent of the bias. Beyond 5 MHz, the capacitance turns negative due to some inductive effect at the interface. A similar observation is reported in the Ni/n-GaAs Schottky diode, where the origin of negative capacitance is attributed to the dominance of deep trap states with longer relaxation times that create a non-ideal phase lag of current leading to an inductive effect [62, 63]. The conductance is bias independent and shoots up after 5 MHz, where capacitance turns negative (see figure 4(c)).

Consistent with the Ag/ScN, Au/ScN diode is also analyzed similarly. From the TE theory, the Schottky barrier height and the ideality factor is calculated to be 0.53 ± 0.06 eV and $\sim$10, respectively. As mentioned earlier, the leakage current in Au/ScN diode is higher than in Ag/ScN. The variation in the *I–V* characteristics with changes in the metal contact size and ageing in Au/ScN diodes are similar to the ones obtained in the Ag/ScN diode. All the *I–V* and *C–V* analysis for Au/ScN is described in the SI section.

The experimental results of the Schottky barrier height are further compared with the Mott–Schottky description of the barrier formation. The barrier height, according to the Mott–Schottky theory, is the difference between the work function of the metal (Φ_m) and electron affinity of the semiconductor ($q\Phi_b = q(\Phi_m - \chi)$) as in figure 1(a). Considering a pure TE, the theoretical and experimental Schottky barrier height for In, Ag and Au on ScN calculated from logarithmic *I–V* plot and Cheung method is presented in table 1. In spite of the 0.5 eV difference in the work function of Ag ($\chi = 4.6$ eV) and Au ($\chi = 5.1$ eV), the almost equal barrier height of Ag/ScN and Au/ScN indicates the possibility of

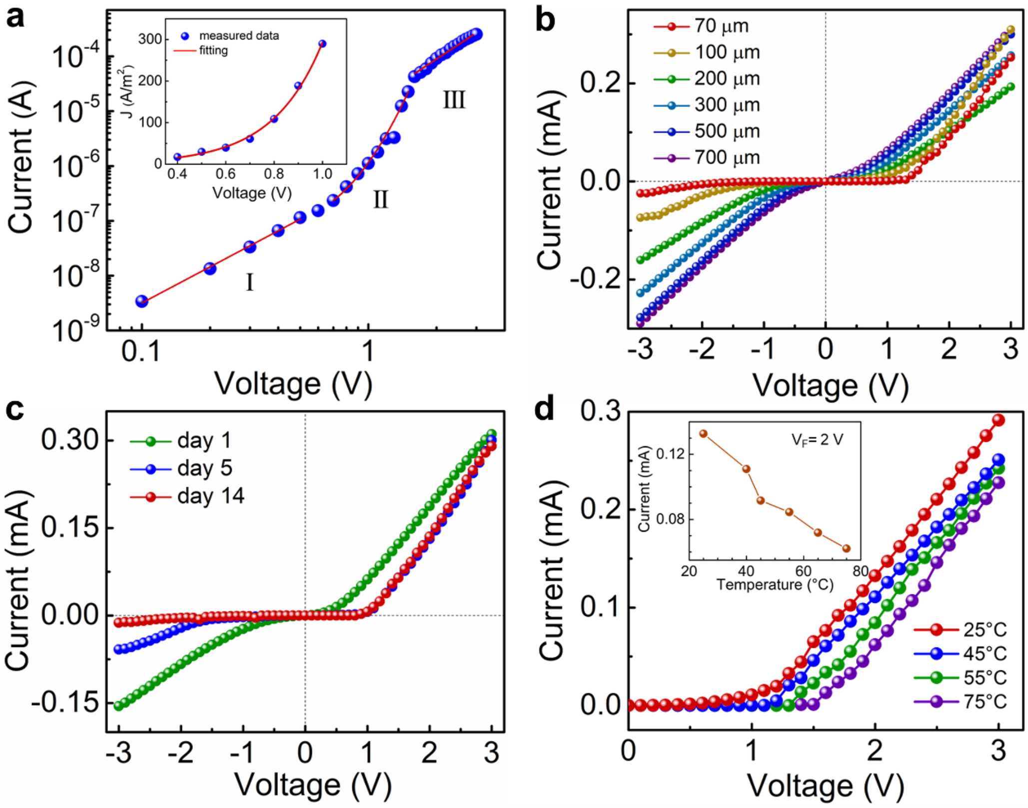

Figure 3. (a) Logarithmic plot of the forward current in the Ag/ScN diode suggests the presence of three regimes of conduction across the barrier. The barrier height of 0.55×0.05 eV is calculated by fitting thermionic equation in regime II as shown in the inset. (b) The reverse current leakage decreases and the rectification is improved for smaller diameters of Ag contacts. (c) *I–V* measured on different days indicate interface reaction leading to better rectification. (d) With increasing temperature, the barrier height slightly increases. The forward voltage drop also increases, and the current at a particular V_F decrease, as in the inset.

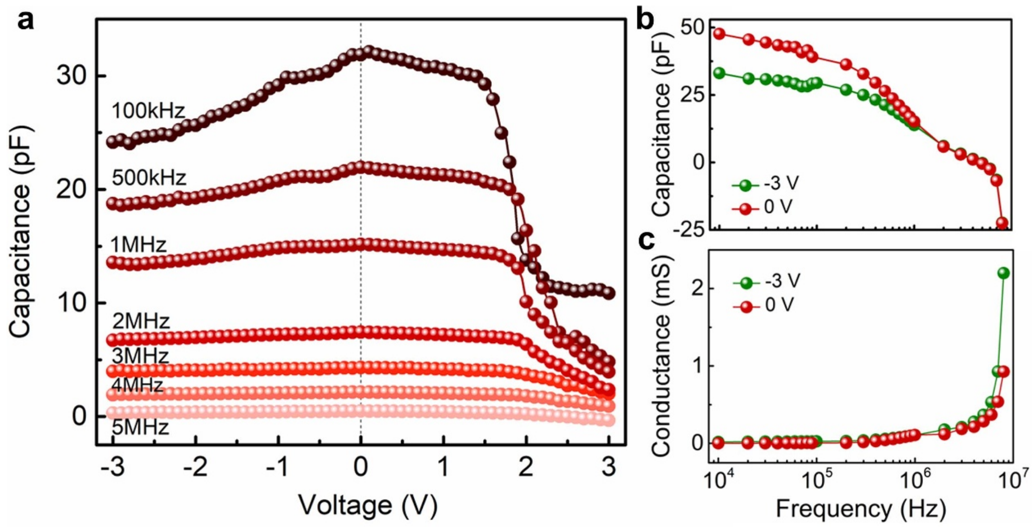

Figure 4. (a) Capacitance–voltage measurement of Ag/ScN indicates the presence of interface trap states whose contribution to the capacitance diminishes at higher frequencies. The presence of interface trap states is also evident in the (b) capacitance–frequency and (c) conductance–frequency curves of Ag/ScN diode.

Fermi-level pinning. The presence of interface states will pin the Fermi level of the semiconductor at the surface before any metal is deposited. Hence, the metal/semiconductor Schottky barrier formation does not follow the Schottky–Mott rule. In such a situation, the band bending in the semiconductor (figure 1(a)) will remain the same for any metal regardless of its work function. Though Mg hole-dopant and oxygen as unintentional donors do not introduce defect states within

Table 1. Comparison of the theoretical and experimental value of the Schottky barrier for In, Ag, and Au. The electron affinity of ScN is 4.1 eV (measured with ultraviolet photoemission spectroscopy (UPS) and will be reported subsequently).

Metal	Φ_m (eV)	Φ_b (eV) (Theory)	Φ_b (eV) (Experimental: log$I$–log$V$)	Φ_b (eV) (Experimental: Cheung)
In	4.1	0	0	0
Ag	4.6	0.5	0.55 ± 0.05	0.54
Au	5.1	1	0.53 ± 0.06	0.47

ScN's bandgap, other types of defects, like dangling bonds at the surface and extended defects, could lead to surface states where Fermi level could pin. Such Fermi-level pinning is quite common among III–V semiconductors, resulting in a specific Schottky barrier height irrespective of the metal [48, 64, 65].

4. Conclusion

In conclusion, Schottky barrier diodes with current rectifying characteristics are demonstrated for the first time in carrier-compensated *n*-type ScN thin films with Ag and Au metallic contacts. With indium as Ohmic contact, non-linear diode-like *I*–*V* curves are obtained for the Ag/ScN and Au/ScN junctions. The average barrier height and ideality factor for Ag/ScN and Au/ScN diodes calculated by fitting the TE equation are 0.55 eV $\pm$ 0.05 eV and 0.53 eV $\pm$ 0.06 eV and 8 and 10, respectively. The rectification improves for smaller contact diameters, presumably due to fewer shunt paths. The Ag/ScN exhibit a much lower leakage current compared to the Au/ScN diode. The barrier height slightly increases with time and temperature, probably due to interfacial modifications. The *C*–*V* measurement indicates the presence of interfacial states whose contribution to capacitance reduces at higher frequencies. Further reduction in electron concentration of ScN, contact size and optimized surface treatment might improve the quality of the diode. This work demonstrates the possibility of achieving a Schottky diode of ScN that paves the way for ScN's application in electronic, thermionic, and optoelectronic devices.

Data availability statement

The data that support the findings of this study are available upon reasonable request from the authors.

Acknowledgments

DR and BS acknowledge International Center for Materials Science (ICMS) and Sheikh Saqr Laboratory (SSL) in JNCASR for support. BS acknowledge Science and Engineering Research Board (SERB) of the Government of India, Start-Up Research grant SRG/2019/000613 for financial support. DR acknowledge Dr Bharath Bannur and Mr. Krishna Chand Maurya for their help in electrical measurements and lithography. DR also acknowledge SAMat. research facilities.

ORCID iDs

Dheemahi Rao https://orcid.org/0000-0002-1952-3210
Shashidhara Acharya https://orcid.org/0000-0001-5145-2427
Bivas Saha https://orcid.org/0000-0002-0837-1506

References

[1] Shah H N 2017 Structural and mechanical characterisation of the chromium nitride hard coating deposited on the silicon and glass substrate *Int. J. Automot. Mech. Eng.* **14** 3872–86
[2] Mayrhofer P H, Rachbauer R, Holec D, Rovere F and Schneider J M 2014 Protective transition metal nitride coatings *Comprehensive Materials Processing* ed S Hashmi, G F Batalha, C J V Tyne and B Yilbas (Oxford: Elsevier) pp 355–88
[3] Kumar D D, Kumar N, Kalaiselvam S, Dash S and Jayavel R 2017 Wear resistant super-hard multilayer transition metal-nitride coatings *Surf. Interfaces* **7** 74–82
[4] Acharya S and Saha B 2019 Epitaxial nitride thin film and heterostructures: from hard coating to solid state energy conversion *Coatings and Thin-Film Technologies* ed J A Perez-Taborda and A G A Bernal (Rijeka: IntechOpen)
[5] Patsalas P, Kalfagiannis N, Kassavetis S, Abadias G, Bellas D V, Lekka C and Lidorikis E 2018 Conductive nitrides: growth principles, optical and electronic properties, and their perspectives in photonics and plasmonics *Mater. Sci. Eng. R* **123** 1–55
[6] Maurya K C, Shalaev V M, Boltasseva A and Saha B 2020 Reduced optical losses in refractory plasmonic titanium nitride thin films deposited with molecular beam epitaxy *Opt. Mater. Express* **10** 2679
[7] Das P, Biswas B, Maurya K C, Garbrecht M and Saha B 2022 Refractory plasmonic hafnium nitride and zirconium nitride thin films as alternatives to silver for solar mirror applications *ACS Appl. Mater. Interfaces* **14** 46708–15
[8] Yuan Y, Wang J, Adimi S, Shen H, Thomas T, Ma R, Attfield J P and Yang M 2020 Zirconium nitride catalysts surpass platinum for oxygen reduction *Nat. Mater.* **19** 282–6
[9] Gall D, Petrov I, Hellgren N, Hultman L, Sundgren J E and Greene J E 1998 Growth of poly- and single-crystal ScN on MgO(001): role of low-energy N +2 irradiation in determining texture, microstructure evolution, and mechanical properties *J. Appl. Phys.* **84** 6034–41
[10] Chowdhury S *et al* 2022 Detailed study of reactively sputtered ScN thin films at room temperature *Materialia* **22** 101375
[11] Dismukes J P, Yim W M and Ban V S 1972 Epitaxial growth and properties of semiconducting ScN *J. Cryst. Growth* **13–14** 365–70
[12] Biswas B and Saha B 2019 Development of semiconducting ScN *Phys. Rev. Mater.* **3** 020301
[13] Oshima Y, Villora E G and Shimamura K 2014 Hydride vapor phase epitaxy and characterization of high-quality ScN epilayers *J. Appl. Phys.* **115** 153508
[14] Gu Z, Edgar J H, Pomeroy J, Kuball M and Coffey D W 2004 Crystal growth and properties of scandium nitride *J. Mater. Sci. Mater. Electron.* **15** 555–9
[15] Saha B, Acharya J, Sands T D and Waghmare U V 2010 Electronic structure, phonons, and thermal properties of ScN, ZrN, and HfN: a first-principles study *J. Appl. Phys.* **107** 033715
[16] Al-Brithen H A, Smith A R and Gall D 2004 Surface and bulk electronic structure of ScN(001) investigated by scanning tunneling microscopy/spectroscopy and optical absorption spectroscopy *Phys. Rev.* B **70** 045303

[17] Casamento J, Wright J, Chaudhuri R, Xing H and Jena D 2019 Molecular beam epitaxial growth of scandium nitride on hexagonal SiC, GaN, and AlN *Appl. Phys. Lett.* **115** 172101

[18] Burmistrova P V, Maassen J, Favaloro T, Saha B, Salamat S, Rui Koh Y, Lundstrom M S, Shakouri A and Sands T D 2013 Thermoelectric properties of epitaxial ScN films deposited by reactive magnetron sputtering onto MgO(001) substrates *J. Appl. Phys.* **113** 153704

[19] Ohgaki T, Watanabe K, Adachi Y, Sakaguchi I, Hishita S, Ohashi N and Haneda H 2013 Electrical properties of scandium nitride epitaxial films grown on (100) magnesium oxide substrates by molecular beam epitaxy *J. Appl. Phys.* **114** 093704

[20] Cetnar J S, Reed A N, Badescu S C, Vangala S, Smith H A and Look D C 2018 Electronic transport in degenerate (100) scandium nitride thin films on magnesium oxide substrates *Appl. Phys. Lett.* **113** 192104

[21] More-Chevalier J, Cichoň S, Horák L, Bulíř J, Hubík P, Gedeonová Z, Fekete L, Poupon M and Lančok J 2020 Correlation between crystallization and oxidation process of ScN films exposed to air *Appl. Surf. Sci.* **515** 145968

[22] More-Chevalier J *et al* 2020 Positron structural analysis of ScN films deposited on MgO substrate *Acta Phys. Pol.* A **137** 209–14

[23] Moram M A, Barber Z H and Humphreys C J 2008 The effect of oxygen incorporation in sputtered scandium nitride films *Thin Solid Films* **516** 8569–72

[24] Kerdsongpanya S, Van Nong N, Pryds N, Žukauskaite A, Jensen J, Birch J, Lu J, Hultman L, Wingqvist G and Eklund P 2011 Anomalously high thermoelectric power factor in epitaxial ScN thin films *Appl. Phys. Lett.* **99** 232113

[25] Rao D *et al* 2020 High mobility and high thermoelectric power factor in epitaxial ScN thin films deposited with plasma-assisted molecular beam epitaxy *Appl. Phys. Lett.* **116** 152103

[26] Tureson N, Van Nong N, Fournier D, Singh N, Acharya S, Schmidt S, Belliard L, Soni A, le Febvrier A and Eklund P 2017 Reduction of the thermal conductivity of the thermoelectric material ScN by Nb alloying *J. Appl. Phys.* **122** 025116

[27] Kerdsongpanya S, Sun B, Eriksson F, Jensen J, Lu J, Koh Y K, Nong N V, Balke B, Alling B and Eklund P 2016 Experimental and theoretical investigation of Cr_{1-x} Sc_xN solid solutions for thermoelectrics *J. Appl. Phys.* **120** 215103

[28] Rao D, Chowdhury O, Pillai A I K, Pradhan G K, Sahoo S, Feser J P, Garbrecht M and Saha B 2022 Multifunctional irradiation-induced defects for enhancing thermoelectric properties of scandium nitride thin films *ACS Appl. Energy Mater.* **5** 6847–54

[29] Burcea R *et al* 2022 Influence of generated defects by Ar implantation on the thermoelectric properties of ScN *ACS Appl. Energy Mater.* **5** 11025–33

[30] Tureson N *et al* 2018 Effect of ion-implantation-induced defects and Mg dopants on the thermoelectric properties of ScN *Phys. Rev.* B **98** 205307

[31] Zywitzki O, Modes T, Barth S, Bartzsch H and Frach P 2017 Effect of scandium content on structure and piezoelectric properties of AlScN films deposited by reactive pulse magnetron sputtering *Surf. Coat. Technol.* **309** 417–22

[32] Eklund P, Kerdsongpanya S and Alling B 2016 Transition-metal-nitride-based thin films as novel energy harvesting materials *J. Mater. Chem.* C **4** 3905–14

[33] Rassay S, Mo D and Tabrizian R 2022 Dual-mode scandium-aluminum nitride lamb-wave resonators using reconfigurable periodic poling *Micromachines* **13** 1003

[34] Moench S *et al* 2022 AlScN-based SAW magnetic field sensor for isolated closed-loop hysteretic current control of switched-mode power converters *IEEE Sens. Lett.* **6** 1–4

[35] Garbrecht M, McCarroll I, Yang L, Bhatia V, Biswas B, Rao D, Cairney J M and Saha B 2020 Thermally stable epitaxial ZrN/carrier-compensated $Sc_{0.99}Mg_{0.01}N$ metal/semiconductor multilayers for thermionic energy conversion *J. Mater. Sci.* **55** 1592–602

[36] Garbrecht M, Schroeder J L, Hultman L, Birch J, Saha B and Sands T D 2016 Microstructural evolution and thermal stability of HfN/ScN, ZrN/ScN, and Hf0.5Zr0.5N/ScN metal/semiconductor superlattices *J. Mater. Sci.* **51** 8250–8

[37] Garbrecht M, Hultman L, Fawey M H, Sands T D and Saha B 2018 Tailoring of surface plasmon resonances in $TiN/(Al_{0.72}Sc_{0.28})N$ multilayers by dielectric layer thickness variation *J. Mater. Sci.* **53** 4001–9

[38] Rawat V, Koh Y K, Cahill D G and Sands T D 2009 Thermal conductivity of (Zr,W)N/ScN metal/semiconductor multilayers and superlattices *J. Appl. Phys.* **105** 024909

[39] Moram M A, Kappers M J, Joyce T B, Chalker P R, Barber Z H and Humphreys C J 2007 Growth of dislocation-free GaN islands on Si(1 1 1) using a scandium nitride buffer layer *J. Cryst. Growth* **308** 302–8

[40] Lupina L, Zoellner M H, Niermann T, Dietrich B, Capellini G, Thapa S B, Haeberlen M, Lehmann M, Storck P and Schroeder T 2015 Zero lattice mismatch and twin-free single crystalline ScN buffer layers for GaN growth on silicon *Appl. Phys. Lett.* **107** 201907

[41] Maurya K C, Rao D, Acharya S, Rao P, Pillai A I K, Selvaraja S K, Garbrecht M and Saha B 2022 Polar semiconducting scandium nitride as an infrared plasmon and phonon–polaritonic material *Nano Lett.* **22** 5182–90

[42] Rao D, Pillai A I K, Garbrecht M and Saha B 2022 Scandium nitride as a gateway III-nitride semiconductor for both excitatory and inhibitory optoelectronic artificial synaptic devices *Adv. Electron. Mater.* 2200975

[43] Ortiz-Libreros M I, Perjeru F, Bai X and Kordesch M E 2001 Investigation of metal contacts on ScN *Appl. Surf. Sci.* **175** 512–6

[44] Perjeru F, Bai X, Ortiz-Libreros M I, Higgins R and Kordesch M E 2001 ScN/GaN heterojunctions: fabrication and characterization *Appl. Surf. Sci.* **175–176** 490–4

[45] Perjeru F, Bai X and Kordesch M E 2002 Electronic characterization of n-ScN/p+ Si heterojunctions *Appl. Phys. Lett.* **80** 995–7

[46] Saha B, Garbrecht M, Perez-Taborda J A, Fawey M H, Koh Y R, Shakouri A, Martin-Gonzalez M, Hultman L and Sands T D 2017 Compensation of native donor doping in ScN: carrier concentration control and p-type ScN *Appl. Phys. Lett.* **110** 252104

[47] Kumagai Y, Tsunoda N and Oba F 2018 Point defects and p-type doping in ScN from first principles *Phys. Rev. Appl.* **9** 34019

[48] Sze S M and Ng K K 2007 *Physics of Semiconductor Devices* (Hoboken, NJ: Wiley)

[49] Nayak S, Baral M, Gupta M, Singh J, Garbrecht M, Ganguli T, Shivaprasad S M and Saha B 2019 Rigid-band electronic structure of scandium nitride across the n-type to p-type carrier transition regime *Phys. Rev.* B **99** 161117

[50] Al-Brithen H and Smith A R 2000 Molecular beam epitaxial growth of atomically smooth scandium nitride films *Appl. Phys. Lett.* **77** 2485–7

[51] Rao D, Biswas B, Acharya S, Bhatia V, Pillai A I K, Garbrecht M and Saha B 2020 Effects of adatom mobility and Ehrlich–Schwoebel barrier on heteroepitaxial growth of scandium nitride (ScN) thin films *Appl. Phys. Lett.* **117** 212101

[52] Lepselter M P and Sze S M 1968 Silicon Schottky barrier diode with near ideal I–V characteristics *Bell Syst. Tech. J.* **47** 195–208
[53] Hacke P, Detchprohm T, Hiramatsu K and Sawaki N 1993 Schottky barrier on n-type GaN grown by hydride vapor phase epitaxy *Appl. Phys. Lett.* **63** 2676–8
[54] Aydin M E and Türüt A 2007 The electrical characteristics of Sn/methyl-red/p-type Si/Al contacts *Microelectron. Eng.* **84** 2875–82
[55] Cheung S K and Cheung N W 1986 Extraction of Schottky diode parameters from forward current-voltage characteristics *Appl. Phys. Lett.* **49** 85–87
[56] Andrews J M and Koch F B 1971 Formation of NiSi and current transport across the NiSi-Si interface *Solid State Electron.* **14** 901–8
[57] Choi Y, Kim Y, Jung E, Oh M and Kim H 2014 Area-dependent electrical characteristics of Schottky diodes fabricated on n-type GaN *J. Korean Phys. Soc.* **64** 1535–8
[58] Taşer A, Güzeldir B and Sağlam M 2017 The stability of electrical characteristics of Ti/n-Si/Ag, Ti/n-Si/Cu and Ti/n-Si/AgCu diodes prepared under the same conditions with respect to increasing aging time *Mater. Sci. Semicond. Process.* **68** 186–92
[59] Vilan A and Cahen D 2017 Chemical modification of semiconductor surfaces for molecular electronics *Chem. Rev.* **117** 4624–66
[60] Kumar A, Kumar A, Sharma K K and Chand S 2019 Analysis of anomalous transport mechanism across the interface of Ag/p-Si Schottky diode in wide temperature range *Superlattices Microstruct.* **128** 373–81
[61] Doğan H, Yildirim N, Orak İ, Elagöz S and Turut A 2015 Capacitance-conductance-frequency characteristics of Au/Ni/n-GaN/undoped GaN Structures *Physica* B **457** 48–53
[62] Bobby A, Shiwakoti N, Verma S, Asokan K and Antony B K 2016 Frequency dependent negative capacitance effect and dielectric properties of swift heavy ion irradiated Ni/oxide/n-GaAs Schottky diode *Physica* B **489** 23–27
[63] Bilkan Ç, Gümüş A and Altindal Ş 2015 The source of negative capacitance and anomalous peak in the forward bias capacitance-voltage in Cr/p-si Schottky barrier diodes (SBDs) *Mater. Sci. Semicond. Process.* **39** 484–91
[64] Spicer W E, Chye P W, Garner C M, Lindau I and Pianetta P 1979 The surface electronic structure of 3–5 compounds and the mechanism of Fermi level pinning by oxygen (passivation) and metals (Schottky barriers) *Surf. Sci.* **86** 763–88
[65] Crowell C R and Sze S M 1966 Current transport in metal-semiconductor barriers *Solid State Electron.* **9** 1035–48